

Research Article

Nanotechnology

Isotretinoin Immobilized on Silica/Ceria Nanoparticles for Optimized Topical Treatment of Acne Vulgaris

Caroline Borges Azevedo¹, Mario Ferreira Conceição Santos¹, Michelle Saltarelli¹, Wilson Rodrigues Braz^{1*}, Arthur Barcelos Ribeiro¹, Mariana Brentini Santiago², Anna Lívia Oliveira Santos²; Emerson Henrique de Faria¹; Eduardo Ferreira Molina¹; Lucas Alonso Rocha¹; Denise Crispim Tavares Barbosa¹; Carlos Henrique Gomes Martins²; Renata Fonseca Vianna Lopez³ and Eduardo José Nassar¹

¹University of Franca; Av. Dr. Armando Salles Oliveira, 201, Pq. Universitário CEP 14404-600. Franca-SP,Brazil ²Federal University of Uberlândia; R. Ceará, S/N, Umuarama CEP 38402-018. Uberlândia-MG, Brazil ³University of São Paulo; Av. Professor Dr. Zeferino, S/N, Campus USP, CEP 14040-903. Ribeirão Preto-SP, Brazil

Abstract:

To treat acne more efficiently, we have synthesized ceria/silica nanoparticles with improved physicochemical and biological properties to enhance topical delivery of isotretinoin. Two types of nanoparticles were synthesized by the sol-gel and co-precipitation methodologies, namely silica containing 10% ceria (SC2 10%) and ceria (C2). SC2 10% and C2 were incorporated with isotretinoin (diluted in dimethylsulfoxide) at a 1:1 (m/m) ratio for 24 h, to give SC2 10%-ISO and C2-ISO, respectively. The nanoparticles had high elemental purity and polydispersity index lower than 0.7. SC2 10% comprised spherical nanoparticles measuring around 300 nm, whereas C2 consisted of agglomerated nanocrystallites with mean diameter ranging from 303 to 515 nm. SC2 10% and C2 had negative (-33.0 mV) and positive (+30.7 mV) zeta potential, respectively. The ISO immobilization efficiency was 11% for SC2 10%-ISO and 16% for C2-ISO, as revealed by indirect quantification by HPLC. An in-vitro drug release study showed that C2-ISO released 16 µg of ISO within 48 h. The cell viability results obtained in HaCat cell culture showed that ISO kept nanoparticle cytotoxicity low, as revealed by XTT assays. Minimum inhibitory concentration assays demonstrated that both SC2 10%-ISO and C2-ISO inhibited Cutibacterium acnes growth, indicating combined action of the drug and nanoparticle matrix. Therefore, ceria-based nanoparticles proved a promising alternative for transporting ISO and promoting its controlled and targeted release: the nanoparticles were chemically stable, presented suitable dispersion characteristics, and inhibited bacterial growth.

Keywords: Silica, Ceria, Isotretinoin, Cytotoxicity, Antibacterial Activity, Nanocarriers

Correspondence:

Wilson Rodrigues Braz, University of Franca; Av. Dr. Armando Salles Oliveira, 201, Pq. Universitário CEP 14404-600. Franca-SP, Brazil, ORCID: 0000-0003-4962-1927;

Received Dates: August 29, 2025; Accepted Date: September 20, 2025; Published Date: September 24, 2025;

> GLOBAL OPEN ACCESS JOURNAL OF SCIENCE

INTRODUCTION

Acne vulgaris, a multifactorial skin condition affecting great part of the human population, commonly occurs during adolescence or even adulthood. Acneic skin is characterized by oily skin and may present with lesions such as comedones, papules, pustules, nodules, and/or cysts. These lesions develop and evolve with proliferation of bacteria, mainly Cutibacterium acnes (previously known as Propionibacterium acnes), which cause inflammatory processes of different severity depending on individual factors, immunological response, and antibody production. The type of lesion and degree of inflammation determine how severe the condition is, and more serious cases may require more elaborate treatment. Grade I acne is characterized by the presence of non-inflammatory comedones (blackheads and whiteheads) only. The emergence of comedones along with inflammation leads to acne being classified into different grades, depending on whether papules (reddish bumps - "internal pimples") and pustules (presence of pus - "pimples") appear or more severe presentations like nodule-cystic lesions arise (Latter et al., 2019; Patel et al., 2020).

Although various acne treatments are available, many patients do not respond to them, especially in the case of severe acne. Isotretinoin (13-cis-retinoic acid, Figure 1a), a synthetic isomer of tretinoin (retinoic acid – the oxidized form of vitamin A, Figure 1b), is usually employed in the oral treatment of severe acne. In milder cases, isotretinoin can be topically applied. This

drug is also used to treat other skin disorders, including rosacea, as well as some forms of neoplastic diseases (Machine *et al.*, 2016; Khalil *et al.*, 2020).

Even though the currently available formulations of isotretinoin as a gel or cream prevent this retinoid from exerting toxicity on vital organs, issues like skin irritation, scaling, and erythema may arise. Furthermore, isotretinoin presents intrinsic physicochemical challenges including instability if exposed to air, light, or heat (Iole et al., 2005; Patel et al., 2011).

To minimize side effects and to improve the topical delivery of anti-acne drugs, nanoparticle systems acting as transporters have been investigated for the targeted delivery of drugs to the pilosebaceous unit, the acne epicenter. These systems stabilize the drug, protect the skin, and reduce side effects. Moreover, these systems allow drugs to be administered at the target tissue in a controlled manner-systems with suitable size facilitate drug penetration into the capillary follicles and provide ideal drug concentration for prolonged time, optimizing therapeutics. Liposomes, niosomes, lipidic and polymeric nanoparticles, nanoemulsions, nanocrystals, nanospheres, quantum dots, inorganic nanoparticles (e.g., silica and calcium phosphate), and solid dispersions have been studied as nanocarriers (Vyas et al., 2014; Chamundesswari et al., 2019; Patel et al., 2020; Gasemiyeh et al., 2020; Roberts et al., 2021).

The approach represents a significant advance over the limitations of conventional acne treatments by

Figure 1: (a) Isotretinoin; (b) Tretinoin.

combining the anti-inflammatory and antioxidant properties of nanoparticles with the clinical repositioning of ISO. The choice of drug and immobilization strategy are in line with current biomedical demands, especially with regard to improving bioavailability, reducing adverse effects, and enabling targeted and non-invasive application, resulting in greater patient compliance with treatment and fewer adverse effects. Therefore, the proposed product has innovative merit and may present a relevant differential in the dermatological therapy scenario.

To reduce the toxicity of isotretinoin and to optimize its therapeutic effects, cerium oxide nanoparticles (or nanoceria) combined with spherical silica nanoparticles have emerged as promising matrixes for carrying this drug. These matrixes offer numerous advantages; for example, they are easy to prepare, present good chemical and thermal stability, are biocompatible, are effectively dispersed in aqueous solution, display antibacterial activity, may act against C. acnes, exhibit anti-inflammatory and antioxidant properties, and strongly absorb UV light, providing the drug with photoprotection.

MATERIALS AND METHODS

Preparation of silica nanoparticles containing 10% ceria

Silica nanoparticles containing ceria were prepared by the non-hydrolytic sol-gel process in ammoniacal medium (Stöber); the adapted methodology described by Azevedo (2014) was followed. Briefly, 1.14 mL of tetraethylorthosilicate alkoxide (TEOS) was mixed with 2.70 mL of deionized water, 15.27 mL of isopropyl alcohol, and 7.88 mL of ammonium hydroxide. Cerium nitrate hexahydrate (0.1 mol L-1, 5.0 mL) was also added at a 10% molar ratio in relation to TEOS. The mixture was magnetically stirred at 60 °C for 4 h, centrifuged at 4000 rpm for 15 min, washed with ethanol three times, and dried at 100 °C. The resulting sample was labeled SC2 10%.

Preparation of ceria nanoparticles

Ceria nanoparticles were prepared by the sol-gel methodology involving chemical co-precipitation with ammonium hydroxide; the methodology adapted from Periyat et al. (2011), was followed. Initially, a 0.1 mol L^1 cerium nitrate hexahydrate solution was magnetically stirred for 30 min. Then, concentrated ammonium hydroxide (30% purity) was added dropwise until pH = 10 was achieved. The resulting solution was continuously stirred at room temperature for 2 h.

The resulting precipitate was collected after centrifugation at 4000 rpm for 15 min, washed, and dried at 100 °C for 12 h. After drying, the yellow solid was dispersed in 100 mL of 0.1 mol L⁻¹ urea solution with pH adjusted to 2.0 by dropwise addition of 3.5 mL of 0.1 mol L⁻¹ hydrochloric acid. The mixture was stirred for 2 h. The resulting solid was separated by centrifugation at 4000 rpm for 15 min, washed with ethanol, and dried at 100 °C. The final sample was labeled C2. The simplified mechanism for the formation of ceria nanoparticles is presented in Equation 1.

$$Ce^{3+} \xrightarrow{NH_4OH} Ce(OH)_4 \xrightarrow{\Delta} CeO_2 - NPs$$
 (1)

Isotretinoin immobilization on the inorganic matrixes SC2 10% and C2

Isotretinoin (ISO) was provided through a collaboration with the Laboratory of Innovation in Nanostructured Systems and Topical Administration, led by Prof. Dr. Renata Fonseca Vianna Lopez of the Faculty of Pharmaceutical Sciences of Ribeirão Preto – University of São Paulo (FCFRP-USP).

ISO was immobilized on an inorganic matrix (SC2 10% or C2) by using the solid matrix dried at 100 °C, so that -OH groups remaining after hydrolysis and condensation could act as drug binding sites. The methodology adapted from Zhao et al. (2017) and Sadhukhan et al. (2019), based on an inorganic matrix/drug 1:1 (m/m) ratio, was followed.

ISO immobilization on SC2 10% or C2 was carried out for 24 h. To this end, a 1 mg mL⁻¹ISO stock solution was prepared by solubilizing 200 mg of ISO in 200 mL of dimethylsulfoxide (DMSO) and stored in the dark. In a round-bottom flask, 100 mL of 1 mg mL⁻¹ISO solution was suspended with 100 mg of SC2 10% or C2. The suspension was sonicated for 20 min with a frequency of 40 kHz and power of 100 W and then magnetically

stirred at room temperature for 24 h, protected from light. After that, the mixture was centrifuged at 4000 rpm for 15 min. The supernatant was collected, and the immobilization efficiency was indirectly determined by HPLC. The final sample containing immobilized ISO (SC2 10%-ISO or C2-ISO), as powder, was dried in a vacuum-drying oven at 60 °C for 24 h.

Physicochemical characterizations

1. Isotretinoin quantification by HPLC coupled to a photodiode array detector: Chromatographic analyses were conducted by using a Shim-pack VP-ODS column (250 mm \times 4.6 mm internal diameter, 5-µm particles; Shimadzu). The isocratic mode was employed, and elution was accomplished by using 80% acetonitrile and 20% water containing 0.1% acetic acid at a flow rate of 1.0 mL min $^{-1}$. The column temperature was kept at 40 °C. The injected volume was 20.0 µL. ISO was detected at a fixed wavelength of 357 nm. The analyses were conducted at the Laboratory of Natural Products of the University of Franca.

2. Immobilization efficiency: The immobilization efficiency (IE %) was determined by quantifying the initial ISO concentration in the stock solution and the free ISO concentration in the supernatant obtained after the colloidal suspension of SC2 10%-ISO or C2-ISO was centrifuged. To quantify ISO in the stock solution, 250 μL of the solution was transferred to a dark flask, to which 750 μL of methanol (HPLC grade) was added. To quantify free ISO, 0.5 mL of the supernatant remaining after ISO immobilization on SC2 10% or C2 was filtered through a 0.45- μm -pore cellulose acetate membrane, and 250 μL of the filtrate was transferred to a dark flask and mixed with 750 μL of methanol. The resulting solutions were analyzed by HPLC. IE% was calculated by using Equation 2:

$$IE\% = \left(1 - \frac{[ISO]supernatant}{[ISO]total}\right) \times 100 (2)$$

where:

[ISO]_{total} total isotretinoin concentration in the stock solution;

 ${\rm [ISO]}_{\rm supernatant}$ free isotretinoin concentration in the supernatant remaining after isotretinoin immobilization on SC2 10% or C2.

3. Zeta potential, hydrodynamic diameter, and

polydispersity index: The size, distribution, and polydispersity index (PdI) of SC2 10%, SC2 10%-ISO, C2, and C2-ISO were evaluated by dynamic light scattering (DLS) on a Nano ZS apparatus operating at 25 °C with scattering angle of 90°. The analyses were conducted by using a 1 mg mL⁻¹ dispersion of the sample in aqueous solution. The zeta potential was determined by laser doppler electrophoresis on this same apparatus. For the analyses, a 1 mg mL⁻¹ dispersion of the sample in a 1 mmol L⁻¹ KCl electrolyte solution was employed. The analyses were performed in triplicate at the Laboratory of Innovation in Nanostructured Systems and Topical Administration of FCFRP-USP.

4. X-Ray diffraction: X-Ray diffraction (XRD) analyses were conducted on a Rigaku Geigerflex D/Max-c diffractometer operating with CuK α radiation (λ = 1.5405 Å) at room temperature. The diffractograms were recorded for 20 ranging from 4 to 80 °, increment of 0.04°, every 10 s. The analyses were carried out at the University of Franca.

5. Infrared absorption spectroscopy: The samples were analyzed by diffuse reflectance infrared absorption spectroscopy (FTIR) on a Perkin Elmer Frontier spectrophotometer; the spectra were recorded from 400 to 4000 cm⁻¹ by using KBr pellets. The analyses were carried out at the University of Franca.

6. UV-Vis absorption spectroscopy: The samples were analyzed on an HP 8453 UV-Vis spectrophotometer operating between 190 and 600 nm. To this end, 1.0 mg of the sample and 2 mL of ethanol were placed in quartz cuvettes with optical path length of 2 mm, and the suspension was sonicated for 30 min. Then, the spectrum was recorded. Pure ISO in ethanol at 31.25 μ g mL⁻¹ was also prepared and analyzed for reference. The analyses were carried out at the University of Franca.

7. Scanning electron microscopy: The samples were deposited on carbon-based adhesive tape, fixed on aluminum stubs, and coated with a thin Au/Pd powder layer in a QUORUM SC7620 Sputter Coater for 120 s. Morphological analyses were conducted on a TESCAN (model VEGA 3 SBH) electron microscope operating with a tungsten filament at 30 kV, resolution of 3.0 nm, and secondary electron (SE) and backscattering electron (BSE) detectors. The amount of sample was sufficient to fill the adhesive tape area, which was approximately 0.5

cm². Sputtering and the morphological analyses were carried out at the University of Franca.

Energy dispersive spectroscopy (EDS) was used to investigate the elemental chemical composition of the samples. For this purpose, a JEOL electron microscope (model JSM-6610LV) with 4.0-nm resolution (30 kV) was employed in the Low Vacuum mode. The samples were deposited on carbon-based adhesive tape and fixed on aluminum stubs, without coating. The analyses were carried out at the Laboratory of Electron Microscopy of the Department of Cell and Molecular Biology of Ribeirão Preto Medical School – University of São Paulo.

8. In-vitro release study: The in-vitro release study was conducted at the Laboratory of Innovation in Nanostructured Systems and Topical Administration of FCFRP-USP. The amount of released ISO was assessed on a Shimadzu UV-1800 UV-Vis spectrophotometer. A calibration curve was constructed from a 500 µg mL⁻¹ ISO stock solution in phosphate buffered saline (PBS)/ ethanol (7:3 v/v). Then, PBS/ethanol (7:3 v/v) was used to prepare ten dilutions from the ISO stock solution, to obtain ISO concentrations of 40, 20, 10, 8, 6, 4, 2, 1, 0.8, and 0.6 µg mL⁻¹. The amount of released ISO was assessed on a Shimadzu UV-1800 UV-Vis spectrophotometer. A calibration curve was constructed from a 500 µg mL⁻¹ ISO stock solution in phosphate buffered saline (PBS)/ ethanol (7:3 v/v). Then, PBS/ethanol (7:3 v/v) was used to prepare ten dilutions from the ISO stock solution, to obtain ISO concentrations of 40, 20, 10, 8, 6, 4, 2, 1, 0.8, and 0.6 µg mL⁻¹. The PBS buffer was prepared by dissolving 40.0 g of NaCl, 1.0 g of KCl, 10.8 g of Na, HPO, .7H, O, and 1.0 g of $KH_{2}PO_{4}$ in 500 mL of water and diluted to 150 mmol L-1. Ethanol was used to solubilize ISO. Absorbance was read at 340 nm. All the points of the calibration curve were prepared and analyzed in triplicate (n = 3). Linearity was determined from the linear regression equation (A = $ax \pm b$) and correlation coefficient (R²). The limits of detection and quantification (LOD and LOQ, respectively) were determined on the basis of the standard deviation of the response (o) and the slope of the analytical curve (S); the equations LOD = $3.3 \sigma/S$ and $LOQ = 10 \sigma/S$ were used.

The specificity of the method was assessed by comparative analyses between the supernatant of SC2 10% or C2 incorporated with ISO or not. Measurements

were carried out in triplicate. For this purpose, an SC2 10%, SC2 10%-ISO, C2, or C2-ISO suspension was prepared by adding 2 mg of the sample to 2 mL of PBS/ethanol (7:3), which was followed by sonication for 1 h. The suspension was allowed to rest in contact with the supernatant for 24 h, protected from light. Next, the suspension was centrifuged at 10,000 rpm for 10 min on a Thermo Fisher Scientific Heraeus Megafuge 16R centrifuge. The supernatant was filtered through 0.45-µm cellulose acetate filter and analyzed on a Shimadzu UV-2550 UV-Vis spectrophotometer operating from 200 to 600 nm.

ISO release from C2-ISO was studied in vitro by following the protocol described by Ogungimi, Chahud and Lopez (2021). Dialysis membranes consisting of cellulose acetate (12-14 kDa, Fisherbrand, Fisher Scientific, EUA) were employed in vertical Franz diffusion cells. The membranes were successively washed with boiling Mili-Q water and remained submerged in Mili-Q water at room temperature until they were used.

In the release system, the membranes were placed between the donor and receptor compartments of the Franz diffusion cells, which had an effective area of 1.2 cm² and volume of 5 mL. The receptor compartment was filled with PBS/ethanol (7:3 v/v) at pH 7.4, which simulated normal physiological conditions. As for the donor compartment, 2 mg of C2-ISO, containing 320 μ g of ISO, in 2 mL of PBS/ethanol (7:3 v/v) was sonicated for 30 min and added to the compartment.

The control consisted of 160 μ g mL⁻¹ ISO solution in PBS/ethanol (7:3 v/v). The diffusion cells were kept under constant stirring at room temperature, protected from light. After certain times (1, 2, 3, 6, 12, 24, and 48 h), 1 mL of the receptor medium was withdrawn for quantification purposes and immediately substituted with an equal volume of standard PBS/ethanol (7:3 v/v). The released ISO concentration was analyzed by UV-Vis absorption spectroscopy at 340 nm. Each preparation was studied in triplicate, and the results are expressed as the mean of the triplicate. The release profile is graphically represented by the percentage of released ISO (%) as a function of time (h).

In this study, the drug release process was investigated by using the Zero-Order, First-Order, Higuchi, and

@2025 Azevedo CB, et al.

Korsmeyer-Peppas mathematical models (Brushi et al., 2015; Mendes et al., 2019). To determine the model better adjusted to the in-vitro release data, the correlation coefficient (R²) was evaluated, so that the value closest to 1 was achieved.

9. Biocompatibility

9.1. Cell viability assessment: A human keratinocyte cell line (HaCat) was employed to evaluate the cytotoxicity of SC2 10%, SC2 10%-ISO, C2, C2-ISO, and free ISO. The cells were cultivated in Dulbecco's Modified Eagle Medium (DMEM; Sigma-Aldrich) supplemented with 10% fetal bovine serum (Nutricell), antibiotics (0.01 mg mL⁻¹ streptomycin and 0.005 mg mL⁻¹ penicillin; Sigma-Aldrich), and 2.38 mg mL⁻¹ Hepes (Sigma-Aldrich) at 37 °C under 5% CO₂. The assays were conducted at the Laboratory of Mutagenesis of the University of Franca.

Cell viability was assessed by an in-vitro toxicology colorimetric assay - Kit XTT (Roche Diagnostics); the manufacturer's guidelines were followed. To perform the assays, HaCat cell suspensions were seeded in 96-well plates at 1.5×10^4 cells/well. After 25 h, the cells were exposed to concentrations of the tested samples ranging from 39.06 to 5000 µg mL⁻¹ in culture medium. Wells containing the negative (untreated cells), solvent (1% DMSO; Sigma-Aldrich), or positive (25% DMSO) control were included.

After incubation at 36.5 $^{\circ}$ C for 24 h, the culture medium was removed, and the cells were washed with 100 μ L of PBS (to remove the tested sample) and exposed to 50 μ L of Ham's Nutrient Mixture F10 (HAM-F10) culture

medium without phenol red (Sigma-Aldrich). Then, 25 μ L of XTT (sodium 3´-{1-[phenylamino)-carbonyl]-3,4-tetrazolium}-bis(4-methoxy-6-nitro) benzenesulfonic acid hydrate) was added to each well.

The microplates were incubated at $36.5\,^{\circ}\text{C}$ for $17\,\text{h}$. The absorbance of the samples was determined by using a microplate reader (ELISA - Asys - UVM 340/MikroWin 2000). Absorbance was read at $450\,\text{nm}$; the reference wavelength was $620\,\text{nm}$. Non-linear regression analyses were carried out by using the GraphPad Prism software to calculate the concentration of the sample that inhibited cell viability by 50% (IC $_{50}$, or half the maximum inhibitory concentration). Figure 2 illustrates the XTT cell viability assay system.

10. Antibacterial activity

10.1. Minimum inhibitory concentration: The Minimum Inhibitory Concentration (MIC) is defined as the lowest concentration of an antimicrobial agent that can inhibit bacterial growth. To determine MIC for SC2 10%, SC2 10%-ISO, C2, C2-ISO, and free ISO against the anaerobic bacterium investigated in this study, the microdilution method recommended by the Clinical and Laboratory Standards Institute (CLSI, 2007), was employed with the modifications described below.

SC2 10%, SC2 10%-ISO, C2, C2-ISO, or free ISO was dispersed in DMSO (Merck°) and diluted in Schaedler (Difco°) broth supplemented with 5 mg mL⁻¹ hemin (Sigma°) and 1 mg mL⁻¹menadione (Sigma°). Next, twelve concentrations of each dispersion varying from 0.98 to 2000 µg mL⁻¹ were tested in 96-well microplates.

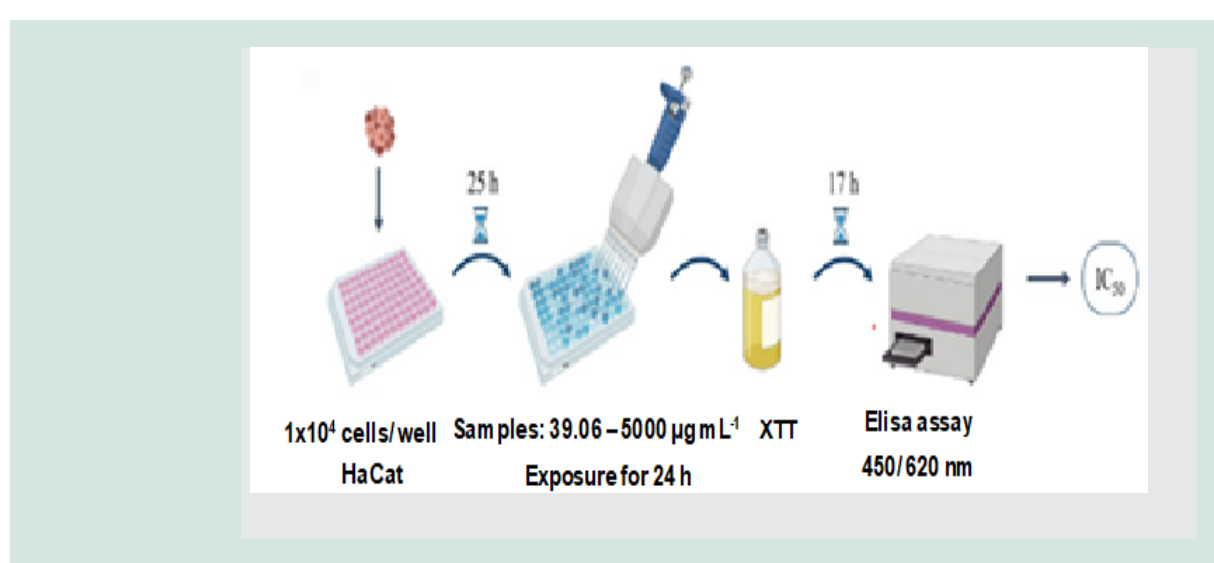


Figure 2: XTT cell viability assay system

The bacterium used in this study was obtained from the American Type Culture Collection (ATCC-USA) – Cutibacterium acnes ATCC 11827. The inoculum was adjusted so that a bacterial concentration of 1×10^6 CFU mL⁻¹ would be achieved.

The anaerobic bacterium was incubated with the tested sample at 37 °C for 72 h in 80% $\rm N_2$, 10% $\rm CO_2$, and 10% $\rm H_2$ in an anaerobic chamber (Don Whitley Scientific, Bradford, U.K.). After incubation, 30 $\rm \mu L$ of aqueous resazurin solution at 0.02 % (Sigma°) was added to the wells, to reveal bacterial growth (Alfenas et al., 2011). The colors blue and pink represent absence and presence of bacterial growth, respectively. DMSO at 5% (v/v) was employed as negative control, and gentamicin (0.0115 to 5.9 $\rm \mu g~mL^{-1}$) was used as positive control. An inoculum control was included to monitor bacterial growth. The assays were performed in triplicate at the Laboratory of Antimicrobial Assays at the Federal University of Uberlândia. Figure 3 shows the MIC assay system.

RESULTS AND DISCUSSION

Isotretinoin quantification by HPLC coupled to a photodiode array detector: The proposed method was selective and linear within the ISO concentration range (20 to 400 μg mL⁻¹) and presented suitable regression coefficient (R² = 0.9943). The LOD and LOQ were 2.0182 and 6.1157 μg mL⁻¹, respectively, indicating that the method was sensitive and adequate for quantifying ISO in all the assays.

Zeta potential, hydrodynamic diameter, polydispersity index, and immobilization efficiency:

It is important to analyze the hydrodynamic diameter distribution (HdD) and zeta potential (ZP) when applying matrixes to carry ISO for topical use. In their reviews, Patel et al. (2020) and Roberts et al. (2021) discussed that an efficient system for topical drug delivery during acne treatment should direct the drug-containing particles to a pilosebaceous unit given that most acne is located on the face, which contains a large quantity of pilous follicles. Furthermore, the concentration of C. acnes, a bacterium playing a crucial role in acne pathogenesis, is high in the sebaceous glands located in this region. Roberts et al. (2021) also highlighted that nanometric particle size, between 300 and 600 nm, would be ideal for the particle to permeate and be retained in the follicle. The smaller the particle, the more efficient its skin permeation and pharmacological action, which should result in fewer side effects on non-target tissues.

Surface charge is another factor that influences the application of nanoparticles in drug delivery. Skin, which has negative ZP, effectively interacts with cationic nanoparticles, that is, nanoparticles with positive ZP. In turn, surface charge improves interaction between the nanoparticle matrix and the stratum corneum as well as pilosebaceous units, to increase the residence time in the target tissue (Wu et al., 2010; Ogunjimi et al., 2021).

Measuring particle size by DLS helps to evaluate the

Table 1: Hydrodynamic diameter (HdD), polydispersity index (PdI), zeta potential (ZP), and immobilization efficiency (IE) of SC2 10%, SC2 10%-ISO, C2, and C2-ISO, presented as the mean ± SD of triplicate analyses.

Sample	HdD (nm)	PdI	ZP (mV)	IE (%)
SC2 10%	303 ± 22	0.138 ± 0.05	-33.0 ± 0.58	-
SC2 10%-ISO	388 ± 8.61	0.343 ± 0.04	-22.6 ± 0.21	11 ± 1.41
C2	515 ± 16.7	0.638 ± 0.14	+30.7 ± 0.06	-
C2-ISO	409 ± 4.7	0.320 ± 0.06	+27.7 ± 0.57	16 ± 0.59

particle HdD in solution. Meanwhile, PdI, a dimensionless value ranging from 0 to 1, is used to measure the particle distribution uniformity. PdI closer to zero indicates more homogeneous and better distributed particles, whereas PdI above 0.7 indicates broad particle size distribution (Rego, 2019).

IE%, obtained by using HPLC to quantify the free drug concentration in the supernatant remaining after the drug was immobilized on the nanoparticle matrix, shows the rate of association between the matrix and ISO. Table 1 lists HdD, PdI, ZP, and IE% of SC2 10%, SC2 10%-ISO, C2, and C2-ISO, expressed as the mean ± standard deviation of triplicate analyses.

On the basis of Table 1, SC2 10%, SC2 10%-ISO, C2, and C2-ISO had nanometric HdD ranging from 303 to 515 nm. Their PdI was below 0.64, indicating that particle size distribution was homogeneous. SC2 10% and C2 exhibited anionic and cationic character, respectively, which was maintained after ISO was immobilized on them.

SC2 10% had HdD of 303 nm and PdI of 0.138, so particle size distribution was highly homogeneous. ZP was negative: -33.0 mV. ZP module above 30 mV suggests that a suspension has electrical stability due to repulsive forces between the particles, so that aggregation is avoided (Ogunjimi, 2018).

After ISO was immobilized on SC2 10%, the ZP module decreased from -33.0 to -22.6 mV. This indicates that the drug and the nanoparticle matrix interact electrostatically (Schaffazick et al., 2003). In turn, HdD

and PdI increased to 388 nm and 0.343, respectively.

C2 had HdB of 515 nm and PdI of 0.638, so particle size distribution was less homogeneous compared to SC2 10%. C2 presented positive ZP, +30.7 mV, attributed to the methodology used in its synthesis, during which HCl was employed to reduce the pH to 2.0 and hence prevent particles from agglomerating. This acidification step was only carried out in the case of C2. According to Firmino et al. (2017), the nanoparticle is protonated under acidic pH, providing C2 with positive charge and thus cationic character.

After ISO was immobilized on C2, ZP varied from +30.7 to +27.7 mV. This indicates that the drug and the nanoparticle matrix were associated. Meanwhile, HdD was 409 nm, and PdI improved to 0.320.

The IE results show that 11% and 16% ISO was immobilized on SC2 10% and C2, respectively. In a study on drug carriers based on mesoporous silica nanoparticles, Guo et al. (2021) also identified low IE for hydrophobic drugs immobilized on the nanoparticles. The fact that ISO is a lipophilic drug accounts for our findings. In addition, Guo et al. (2021) reported that IE is influenced by ZP of the nanoparticle matrix and drug. The authors observed that nanoparticles and drugs with opposite charges have increased IE, as observed here for C2-ISO (IE = 16%).

When Braz et al. (2016) incorporated indometacin, an anti-inflammatory drug, into mesoporous silica, IE was 7%. Cytotoxicity tests conducted on normal fibroblast cells (GM0479A) indicated that the incorporated drug

Table 2: Vibrational modes of ISO, SC2 10%, SC 10%-ISO, C2, and C2-ISO.

Vibrations	ISO	SC2	SC2 10%	C2	C2
	(cm ⁻¹)	-10%	-ISO	(cm ⁻¹)	-ISO
		(cm ⁻¹)	(cm ⁻¹)		(cm ⁻¹)
δ (Si-O-Si)	-	476	466	-	-
υ(Ce-0)	-	-	-	411-632	411-
					632
υ(Si-OH)	-	954	951	-	-
$v_{as}(Si-O-Si)$	-	1106	1106	-	-
υ(<i>C-0</i>)	1350	-	1317	-	1332
υ(C=O)	1673	-	1664	-	1628
$v_{as}(C-H)$	2927	-	3000	-	2928
υ(<i>0-H</i>)	_	3242	3249	3423	3268

was less toxic than the free drug. Therefore, low IE may be beneficial when it comes to delivering a sufficient and non-toxic drug dose at the target tissue.

Together, our findings show that both SC2 10% and C2 have suitable size for application as nanocarriers. Besides that, all the nanoparticle dispersions present high ZP, which benefits stability. That ISO is indeed associated with the nanoparticle matrix was evident from the fact that ZP changed after immobilization.

C2 having positive ZP may have led to a higher affinity between this nanoparticle matrix and the skin surface. This is advantageous because skin interacts more favorably with cationic particles.

3.3. X-ray diffractometry. The XRD patterns of SC2 10% and C2 helped to investigate the structure of isolated ceria and ceria interacting with silica. Figure 4 shows the XRD patterns of SC2 10%, C2, and ceria standard (JCPDS 1-800) dried at 100 °C.

The XRD pattern of C2 was consistent with the fluorite cubic structure, typical of ceria (Figure 4, black line), as evidenced by the Bragg peaks at $2\theta = 28$, 33, 47, 56, 59, 69, and 76°. These peaks correspond to the Miller indices (111), (200), (220), (311), (222), (400), and (331), respectively, and attest to the crystalline purity of C2. Features of other phases were not evident (Kargar et al., 2015; Fereydouni et al., 2018; Nourmohammadi et al., 2018; Sharmila et al., 2019).

We calculated the mean crystallite size by using the Scherrer equation (Equation 3):

$$D(nm) = \frac{\kappa\lambda}{\beta\cos\theta} (3)$$

where:

D = crystallite size (nm);

ß = full width at half height of the most intense
diffraction peak;

 Θ = Bragg angle;

K = Scherrer constant, whose value depends on crystallite shape. In this case, we adopted a value of 0.9, which corresponds to the spherical crystallite shape.

The crystallites had mean diameter of 11 nm. The XRD pattern of SC2 10% dried at 100 °C displayed halos typical of amorphous silica and a broad peak at $2\theta = 22^{\circ}$ (Zhang et al., 2022). The absence of XRD diffraction peaks suggests that ceria remained dispersed in the silica matrix during the sol–gel synthesis, so that crystalline CeO₂ was not formed.

Infrared absorption spectroscopy

The FTIR spectra helped to evaluate the chemical properties of free ISO and its interactions with SC2 10% and C2. Table 2 summarizes the vibrational modes of ISO, SC2 10%, SC2 10%-ISO, C2, and C2-ISO.

ISO bears five conjugated double bonds and a -COOH group in its end. Its FTIR spectrum displayed absorption bands in the regions of interest. The band at 2927 cm⁻¹ corresponds to aliphatic -CH bond stretching, whereas the bands at 1673 and 1599 cm⁻¹ are due to carboxylic acid C=O and C=C bond stretching, respectively. The intense band at 1250 cm⁻¹ refers to -OH group stretching vibration (Zhao et al., 2017; Khalil et al., 2020).

On the basis of Table 2, the FTIR spectrum of SC2 10% displayed the typical bands of silica [33], i.e., the

Table 3: Minimum inhibitory concentration (MIC) of C2, C2-ISO, SC2 10%, SC2 10%-ISO, or free ISO, in μ g mL⁻¹, against *Cutibacterium acnes.*

Sample	Cutibacterium acnes		
	ATCC 11827		
SC2 10%	500		
SC2 10%-ISO	7.8		
C2	1000		
C2-ISO	7.8		
Free ISO	3.9		
Gentamicin (control)	0.37		

Samples solubilized in DMSO

Sample concentrations varied from 0.98 to 2000 $\mu g\ mL^{\text{-}1}$

Gentamicin concentrations varied from 0.0115 to 5.9 µg mL⁻¹

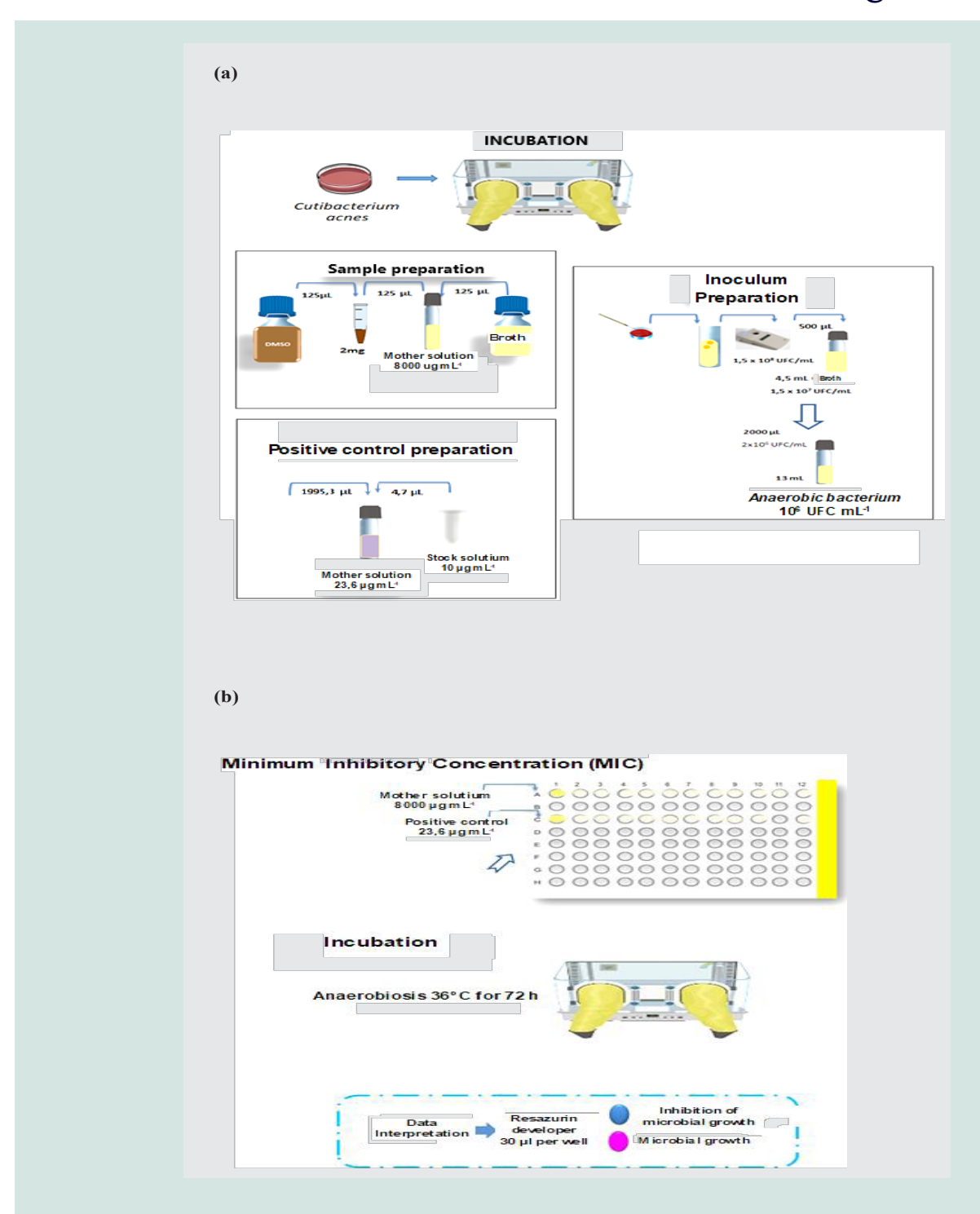


Figure 3: Minimum Inhibitory Concentration (MIC) assay system: (a) Incubation, sample, positive control, and inoculum preparation; (b) incubation and data interpretation.

 $\upsilon_{as}(Si\text{-O-Si})$, $\upsilon_{s}(Si\text{-O-Si})$, and $\delta(Si\text{-O-Si})$ vibrational modes emerged at 1106, 800, and 476 cm⁻¹, respectively. Besides that, absorption bands related to (Si-OH) silanol groups appeared at 3642 and 954 cm⁻¹, indicating that these groups were not totally condensed. The presence of adsorbed water on the surface was clear from the emergence of a broad band with maximum absorption around 3242 cm⁻¹, as well as a band around 1627 cm⁻¹

 1 , corresponding to the $\upsilon(\text{O-H})$ vibrational mode of water molecules (bound through H) and water $\delta(\text{OH})$ angular deformation, respectively. The small bands in the regions of 1400 and 2983 cm $^{-1}$ can be attributed to symmetric and asymmetric deformation of C-H bonds and indicate the presence of organic matter (Khalil et al., 2005; Azevedo et al., 2015; Braz et al., 2016; Pawlaczyk et al., 2019).

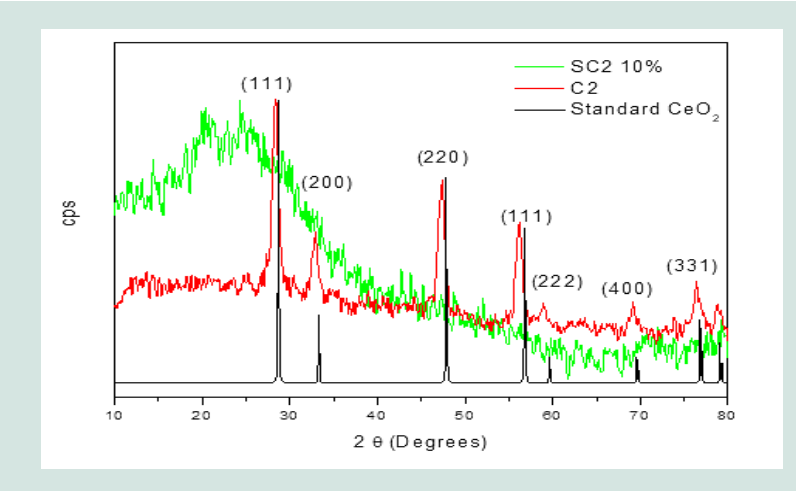


Figure 4: X-ray diffraction pattern of SC2 10% (green), C2 (red), and the ceria standard (black), dried at 100 °C.

Comparison between the vibrational modes of free ISO and SC2 10%-ISO shows that the FTIR spectrum of the latter sample displayed the characteristic absorption bands of silica, as well as three less intense bands around 317, 1414, and 1664 cm⁻¹, ascribed to C-O and C-H bond stretching of ISO C=O, respectively. Although the IE calculated by HPLC was low, the drug was detected in SC2 10%. (Viossat et al., 2005; Zhao et al., 2017; Matos, 2021).

As for the FTIR spectrum of C2, the band due to Ce-O bond stretching arose between 411 and 632 cm⁻¹ and peaked at 428 cm⁻¹. The broad bands at 3320 and 1637 cm⁻¹ can be assigned to residual water and Ce-OH groups, respectively (Fereydouni et al., 2018).

Concerning the FTIR spectrum of C2-ISO, it contained bands typical of CeO₂, as well as bands indicating the presence of organic matter. This shows that ISO interacted with C2. More specifically, the bands emerged at 1332, 1408, 1564, and 2928 cm⁻¹. The band due to free

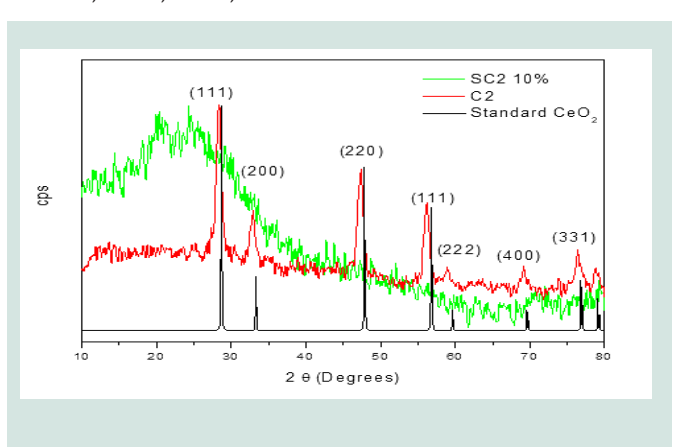


Figure 5: UV-Vis spectra of SC2 10% (black) and C2 (red).

carboxylic acid υ(C=O) stretching at 1673 cm⁻¹ in the FTIR spectrum of free ISO shifted to lower wavenumber in the FTIR spectrum of C2-ISO and was unfolded into two new bands, at 1564 and 1332 cm⁻¹, referring to (COO⁻) asymmetric and symmetric stretching (Yap et al., 2005; Zhao et al., 2017). According to Viossat et al. (2005), this unfolding occurs after carboxylate forms a complex with metal centers. The absorption bands due to asymmetric and symmetric (C-H) stretching appeared at 2928 and 1408 cm⁻¹, while the broad band corresponding to hydration water peaked at 3320 cm⁻¹. These results indicate that ISO and C2 interact in C2-ISO (Yap et al., 2005; Viossat et al., 2005; Zhao et al., 2017).

UV-Vis absorption spectroscopy

UV-Vis absorption spectroscopy helped to characterize SC2-10% and C2 and to detect ISO in the nanoparticle matrixes. Figure 5 shows the UV-Vis spectra of SC2-10% and C2.

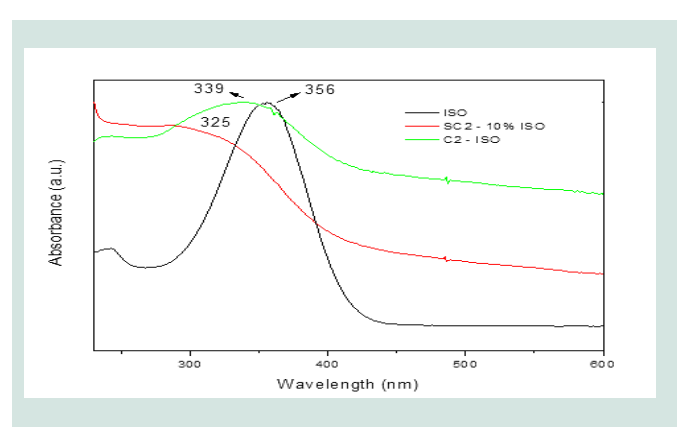


Figure 6: UV-Vis spectra of free ISO (black), SC2 10%-ISO (red), and C2-ISO (green).

@2025 Azevedo CB, et al.

According to the literature Barrie et al.(1990) and Bensalem et al. (1995), the bands at 233 and 297 nm are due to Ce³⁺ interconfigurational 4f–5d transitions and were previously observed in the UV-Vis spectrum of alumina doped with ceria. The UV-Vis spectrum of C2 displayed a broad band between 250–350 nm, which peaked at 233 and 297 nm, suggesting the presence of Ce³⁺.

The SC2 10% UV-Vis spectrum evidenced a shift toward the red, attributed to $O^{2-} \rightarrow Ce^{4+}$ charge transfer. This shift suggests the presence of two species, Ce^{3+} and Ce^{4+} (Zaki et al., 2017; Sharmila et al., 2019; Sandrini et al., 2023). These two oxidation states of cerium (III and IV) generate structural defects with oxygen vacancies, which leads to absorption at various wavelengths and broadens the absorption band (Eduardo et al., 2021; Gao et al., 2021).

The Figure 6 shows the UV-Vis spectra of ISO, SC2 10%-ISO, and C2-ISO. SC2 10%-ISO and C2-ISO at 500 μ g mL⁻¹ were suspended in ethanol and sonicated for 30 min before the spectra were recorded.

The UV-Vis spectrum of free ISO displayed an intense band at 356 nm, which corresponds to the $\pi \to \pi^*$ transition in the conjugated polyene structure of ISO. This agrees with the wavelength identified for ISO by HPLC (Machine et al., 2016; Zhao et al., 2017).

The absorption bands at 325 and 339 nm in the UV-Vis spectra of SC2 10%-ISO and ISO-C2, respectively, can be attributed to interactions between ISO and the nanoparticle matrix (Chinnu et al., 2013; Luo et al., 2020). Confirming the shifts in the carbonyl peaks observed in the corresponding FTIR spectra. This suggests that ISO coordination to the matrix surface did not affect the

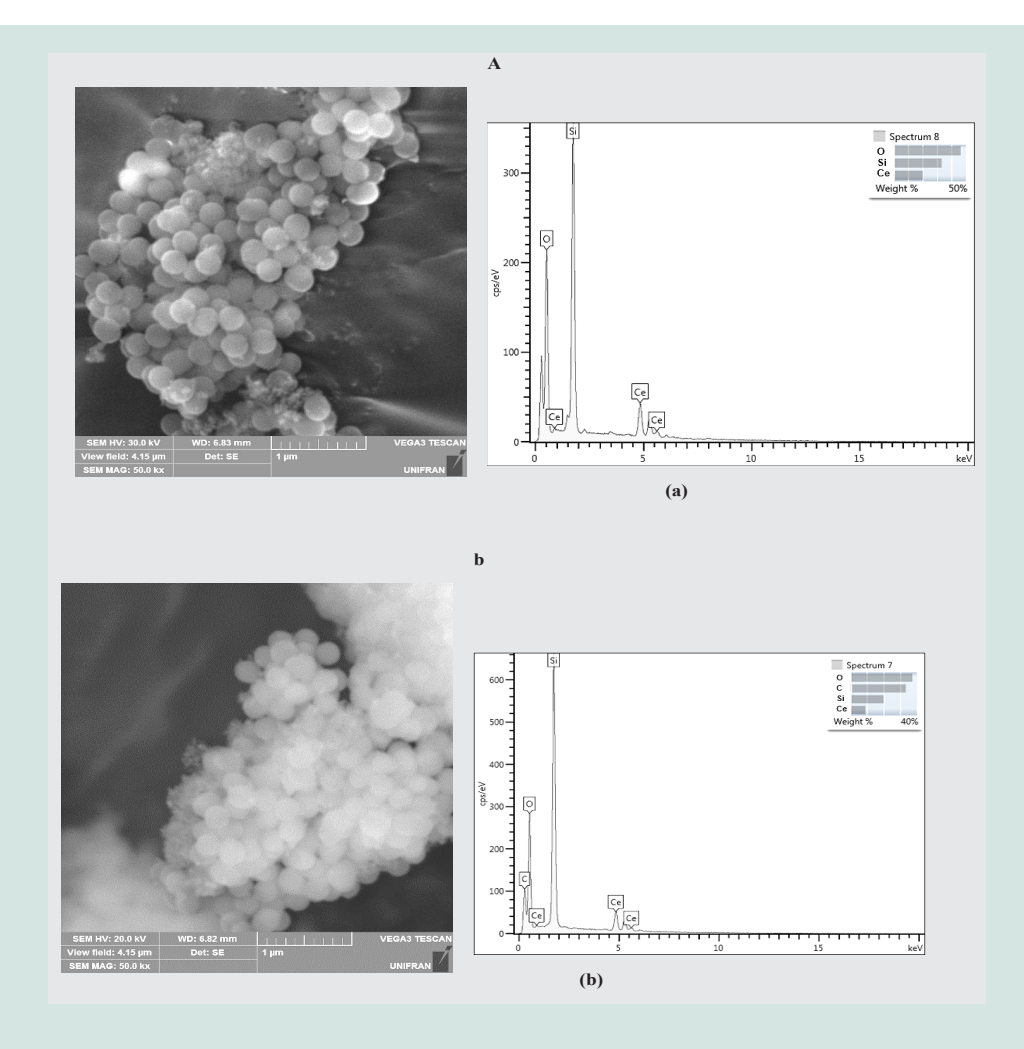


Figure 7: SEM images and EDS spectra of (a) SC2 10% and (b) SC2 10%-ISO at 50,000 magnification.

physicochemical stability of the nanoparticle matrix.

Research conducted by Zholobak et al. (2020) on ceria nanocomposites with curcumin revealed that the ceria nanoparticles reduce curcumin degradation in aqueous solutions. This indicates that SC2 10% and C2 are promising matrixes for drug transport, and that they protect the drug structure.

Scanning electron microscopy:

We investigated the morphology and chemical composition of SC2 10% and C2 by SEM before and after ISO incorporation. Figure 7 (a and b) shows the scanning electron microscopy (SEM) images and EDS spectra of SC2 10% and SC2 10%-ISO.

The SEM images recorded before and after ISO was incorporated into SC2 10% did not reveal considerable morphological alterations. Dense, agglomerated spherical particles measuring around 300 nm were formed. This size is compatible with the HdD of the nanoparticles (Table 1). Indeed, we had expected that the synthesis methodology would provide spherical particles, as described by Azevedo et al. (2015).

The EDS spectra revealed that silicon and oxygen were the main components of the nanoparticles. Cerium at 10%, added during the synthesis, was also present. The peak due to carbon could be due to the organic molecule ISO or the carbon tape used in the sample holder. Figure 8 (a and b) shows the SEM images and EDS spectra of C2 and C2-ISO.

The SEM images of C2 showed that nanoparticle agglomerates emerged. The particles were irregular, and their size was in the order of micrometers. On the basis of the Scherrer equation, the crystallite size was estimated as 11 nm. This suggests that ceria nanoparticles tend to agglomerate.

The EDS spectra identified that cerium and oxygen were the main components of the nanoparticles, which indicated matrix purity. The peak due to carbon could be due to the organic molecule ISO or the carbon tape used in the sample holder.

Cell viability

In-vitro cell viability and cytotoxicity assays involving cultured cells are widely employed to test the cytotoxicity of chemical products and to screen drugs. The principle

underlying the MTT (3-(4,5-dimethyl-2-thiazolyl)-2,5diphenyl-2H-tetrazolium bromide) and XTT assays is to measure a biochemical marker (tetrazolium salt) with a specific color. This is possible because the reduction reaction provoked by the metabolic activity of cell membrane mitochondria generates a colored formazan product (Aslanturk, 2018). The main difference between the MTT and XTT assays is that the former produces a purple formazan that is insoluble in water, whereas the latter generates orange formazan crystals that are soluble in the culture medium. The XTT assay requires fewer steps, so it is more advantageous than the MTT assay. The intensity of the orange color emitted by the formazan salt is measured on a spectrophotometer or ELISA reader. The more intense the orange color, the greater the number of viable cells in the well (Aslanturk, 2018; Rajeshkumar et al., 2018). Figure 9 presents the viability cell plot obtained during the XTT colorimetric assay conducted for HaCat cells exposed to SC2 10%, SC2 10%-ISO, C2, C2-ISO, or free ISO concentrations varying from 39.06 to 5000 ug mL⁻¹.

HaCat cells treated with free ISO concentrations varying from 153.3 to 5000 μg mL⁻¹ for 24 h presented reduced cell viability. Interestingly, HaCat cells treated with the highest SC2-10% and C2 concentrations also had 15% lower cell viability. However, C2, C2-ISO, SC2 10%, SC2 10%-ISO, or ISO at the tested concentrations were not notably cytotoxic. Nourmohammadi et al. [29] also synthesized ceria nanoparticles with satisfactory cell viability concerning the WEHI 164 cell line, as revealed by the MTT colorimetric assay. Thus, these nanoparticles can potentially be applied in numerous biomedical areas.

Cytotoxicity remained low after ISO was incorporated into the nanoparticle matrixes, irrespective of the drugmatrix concentration. Considering that 1250 μg of C2-ISO and SC2-ISO contain 200 μg (IE% = 16%) and 135.5 μg (IE% = 11%) of ISO, respectively, the presence of the nanoparticle matrix reduced ISO toxicity probably because the drug was sustainably released in the medium at a non-cytotoxic dosage. Therefore, on the basis of the XTT colorimetric assay involving HaCat cells, the nanoparticles prepared herein are excellent candidates for biological use.

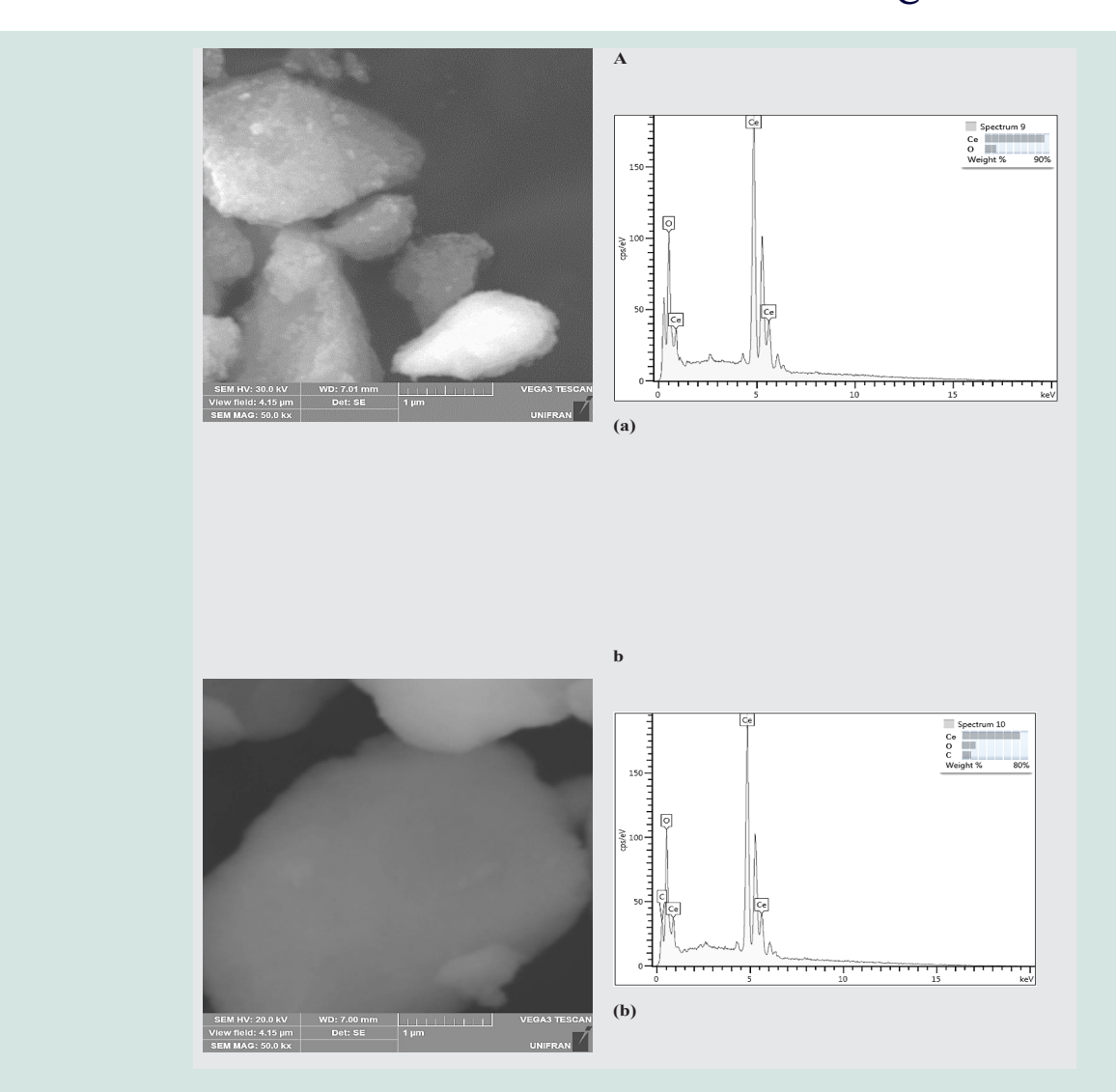


Figure 8: SEM images and EDS spectra of (a) C2 and (b) C2-ISO at 50,000 magnification

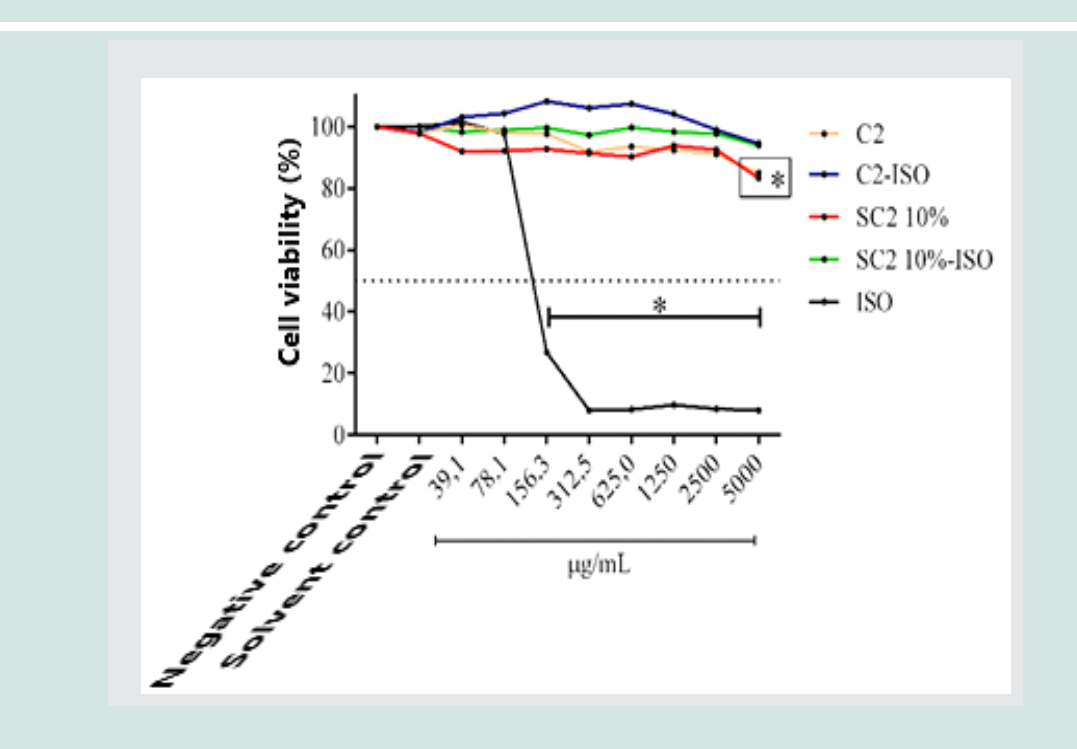


Figure 9: Cell viability in culture medium of HaCat treated with C2, C2-ISO, SC2 10%, SC2 10%-ISO, or free ISO at different concentrations (39.06–5000 μg mL⁻¹) for 24 h.

Antibacterial effect of the nanoparticles containing isotretinoin or not

1 Minimum inhibitory concentration: MIC determination helped to study the antibacterial effect of C2, C2-ISO, SC2 10%, SC2 10%-ISO, or ISO at concentrations ranging from 0.98 to 2000 μ g mL⁻¹ against C. acnes ATCC 11827, a Gram-positive and anaerobic bacterium. Table 3 lists the results.

Free ISO displayed antibacterial activity (MIC = $3.9 \mu g$ mL⁻¹0, whereas gentamicin provided MIC of $0.37 \mu g$ mL⁻¹. SC2 10% and C2 at 500 and 1000 μg mL⁻¹, respectively, without the drug, inhibited bacterial growth.

In a review about the biomedical applications of ceria nanoparticles, Rajeshkumar et al. (2018) reported that nanoceria can inhibit the action of aerobic bacteria, including Pseudomonas aeruginosa (NCIM-2242). Inhibition occurred for nanoceria concentrations ranging between 500 and 1000 μg mL⁻¹ during the agar well diffusion method (well technique) and between 200 and 400 μg mL⁻¹ during the broth dilution method. According to the authors, the mechanism underlying the antibacterial activity involves reactive oxygen species (ROS).

Studies have described the antibacterial action of ceria nanoparticles and cerium-based nanomaterials (composites or doped materials), mostly against Escherichia coli and Staphylococcus aureus (Wang et al., 2018; Pop et al., 2020; Latif et al., 2021).

Regarding C. acnes, SC2 10% had higher antibacterial activity than C2. According to Firmino et al. (2017), the mechanisms underlying the antibacterial action of ceria are unclear, but the most accepted mechanisms involve contact of the nanoparticle matrix with the bacterial cell membrane and oxidative stress. For the matrix to interact with the bacterial cell membrane, the nanoparticle charge must be opposite the surface charge of the bacterial cell, to favor electrostatic interactions. Bacteria generally have negative surface charge (Frade et al., 2018). Oxidative stress stems from alternated oxidation states (Ce³⁺/Ce⁴⁺), to generate ROS. The lower the Ce³⁺/Ce⁴⁺ ratio, the higher the antibacterial activity. Other factors affecting the antibacterial activity of nanoparticle matrixes include particle size, surface area, morphology, ZP, pH, and particle aggregation

(Firmino et al., 2017).

Although SC2 10% nanoparticles bear negative charge (negative ZP), they measure around 300 nm, present good dispersion, are spherical, and thus have larger surface area. These factors may have favored the antibacterial action of SC2 10% compared to C2.

After ISO was incorporated into SC2 10% or C2, MIC decreased to 7.8 µg mL¹ in both cases, which indicated that the antibacterial activity improved, that is, the combined action of ISO and the nanoparticle matrix decreased MIC against C. acnes. Besides that, SC2 10% and C2 reduced the ISO cytotoxicity, as revealed by the cell viability assays. Therefore, incorporated ISO displayed antibacterial activity without affecting cell viability.

Overall, it is evident that nanoparticles are an important vehicle for targeted delivery of ISO and derivatives. ISO incorporated into nanoparticles has good biological properties and fewer adverse effects than free ISO. In conclusion, SC2 10% and C2 proved promising for such application, but C2 has greater drug stabilization ability, being more interesting for drug delivery purposes.

CONCLUSIONS

A challenging and relevant research field is to obtain nanoparticles that can prevent direct contact of isotretinoin (ISO) with the skin. In this way, ISO delivery can be directed toward the target site while side effects are reduced and topical treatment of acne vulgaris is improved. Here, we have shown that the synthesis of silica and ceria nanoparticles (SC2 10%) by the solgel methodology in ammoniacal medium and of ceria nanoparticles (C2) by the sol-gel methodology and coprecipitation is satisfactory. The synthesis provided highly pure nanoparticles with suitable particle size (between 300 and 500 nm), polydispersity index, and electrical properties for the intended application, as revealed by hydrodynamic diameter, zeta potential, scanning electron microscopy (SEM), energy dispersive spectroscopy, and X-ray diffraction analyses. The SEM images showed that SC2 10% consist of spherical nanoparticles, and that C2 comprise nanoparticle agglomerates.

ISO immobilization on SC2 10% or C2 was quantified by

HPLC. The adopted method was adequate and allowed the immobilization efficiency (IE) to be quantified by analyzing the ISO concentration in the supernatant of the colloidal solution remaining after immobilization. The different IE% determined for SC2 10% (11%) and C2 (16%) are related to nanoparticle charge and ISO lipophilicity. ISO has higher affinity for cationic C2. Despite low IE, C2 provide sustained ISO delivery (16 μ g) within 48 h.

UV-Vis and infrared spectroscopy attested to successful ISO immobilization on C2. C2 stabilize the drug, while SC2 10% oxidize ISO.

The infrared band assignments for SC2 10%-ISO and C2-ISO confirmed the immobilization efficiency. The zeta potential values showed that C2 interact more strongly with ISO, as judged from the better-defined infrared bands verified for ISO immobilized on C2.

The cell viability results obtained during the XTT assays involving HaCat showed that SC2 10% and C2 are biocompatible and reduce ISO cytotoxicity. Even after ISO degradation was detected for SC2 10%-ISO, the antibacterial activity of immobilized ISO proved satisfactory and showed that combining the properties of the drug and SC2 10% or C2 improves the antibacterial

activity of ISO as verified by the minimum inhibitory concentration assays. Thus, in the future, SC2 10% could be tested in combination with other drugs.

To sum up, the nanoparticles matrixes developed herein are promising for the advance of drug nanocarriers. Nanoceria stands out as a potential ISO carrier, paving the way for more efficient acne treatment.

ACKNOWLEDGEMENTS

The authors thank funding by Fundação de Amparo à Pesquisa do Estado de São Paulo (FAPESP) – Process number 2019/20777-6 C.B.A. and 2019/26439-5 E.J.N.; Coordenação de Aperfeiçoamento de Pessoal de Nível Superior (CAPES) – Finance Code 001; and Conselho Nacional de Desenvolvimento Científico e Tecnológico (CNPq) – Process number 308983/2021-1 L.A.R. and 303228/2021-0 E.J.N. The authors also thank the Laboratory of Mutagenesis at UNIFRAN; the Laboratory of Natural Products at UNIFRAN; the Laboratory of Innovation in Nanostructured Systems and Topical Administration at FCFRP-USP; the Laboratory of Antimicrobial Assays at UFU; the University of São Paulo – campus in Ribeirão Preto, SP; and the Federal Institute – campus in Catanduva, SP.

REFERENCES:

 Adan. A., Kiraz, Y., & Baran, Y. (2016). Cell proliferation and cytotoxicity assays. Current pharmaceutical biotechnology, 17:14 1213-1221

DOI: https://doi.org/10.2174/1389201017666160808160513

• Alfenas, C. S., Ricci, G. P., Faria, E. H., Saltarelli, M., Lima, O. J., Rocha, Z. N., Nassar, E. J., Calefi, P. S., Montanari, L. B., Martins, C. H. G., & Ciuffi, K. J. (2011). Antibacterial activity of Nb-aluminum oxide prepared by the non-hydrolytic sol-gel route. *Journal of Molecular Catalysis A: Chemical*, 338(1–2), 65–70.

DOI: https://doi.org/10.1016/j.molcata.2011.01.026

• Aslanturk, O. S. (2018). In vitro cytotoxicity and cell viability assays: principles, advantages, and disadvantages. In *Genotoxicity – A predictable risk to our actual world*, 2(64–80).

DOI: https://doi.org/10.5772/intechopen.71923

- Azevedo, C. B. (2014). Preparação e caracterização de materiais híbridos luminescentes pelo método sol-gel em meio amoniacal. *Dissertação (Mestrado em Ciências)*, Universidade de Franca, Franca.
- Azevedo, C. B., Batista, T. M., De Faria, E. H., Rocha, L. A., Ciuffi, K. J., & Nassar, E. J. (2015). Nanospherical silica as luminescent markers obtained by sol-gel. *Journal of Fluorescence*, 25(2), 433–440.

DOI: https://doi.org/10.1007/s10895-015-1530-4

 Barrie, J. D., Momoda, L. A., Dunn, B., Gourier, D., Aka, G., & Vivienz, D. (1990). ESR and optical spectroscopy of Ce³⁺: β"-Alumina. *Journal of Solid State Chemistry*, 86(1), 94–100.

DOI: https://doi.org/10.1016/0022-4596(90)90118-H

- Bensalem, A., Bozon-Verduraz, F., Delamar, M., & Bugli, G. (1995). Preparation and characterization of highly dispersed silica-supported ceria. *Applied Catalysis A: General*, 121, 81–93.
 - DOI: https://doi.org/10.1016/0926-860X(95)85012-0
- Braz, W. R., Rocha, N. L., De Faria, E. H., Silva, M. L. A., Ciuffi, K. J., Tavares, D. C., Furtado, R. A., Rocha, L. A., & Nassar, E. J. (2016). Incorporation of anti-inflammatory agent into mesoporous silica. *Nanotechnology*, 27, 385103 (1–9).
 - DOI: https://doi.org/10.1088/0957-4484/27/38/385103
- Bruschi, M. L. (2015). Strategies to modify the drug release from pharmaceutical systems. *Woodhead Publishing*, 199p.
- https://www.sciencedirect.com/book/9780081000922/strategies-to-modify-the-drug-release-from-pharmaceutical-systems
- Chamundesswari, M., Jeslin, J., & Verma, M. L. (2019). Nanocarriers for drug delivery applications. *Environmental Chemistry Letters*, 17(2), 849–865.
 - DOI: https://doi.org/10.1007/s10311-018-00841-1
- Chinnu, M. K., Anand, K. V., Kumar, R. M., Alagesan, T., & Jayavel, R. (2013). Synthesis and structural, optical and thermal properties of ceria and rare earth doped ceria nanocrystals. *Optoelectronics and Advanced Materials Rapid Communications*, 7(11–12), 976–979.
 - DOI: https://www.researchgate.net/publication/261951624
- CLSI. (2007). Methods for Antimicrobial Susceptibility Testing of Anaerobic Bacteria; Approved Standard-Seventh Edition. *Clinical and Laboratory Standards Institute*, 27(2).
- Eduardo, A. C., Rodrigues, M. H. M., Mesquita, W. D., Gonçalves, R. F., Gurgel, M. F. C., & Godinho, M. J. (2021).
 Estudo da degradação do pesticida fipronil utilizando heteroestruturas de semicondutores de BiVO₄/CePO₄ e
 CePO₄/BiVO₄. Cerâmica, 67(384), 455–462.
 - DOI: https://doi.org/10.1590/0366-69132021673843082
- Fereydouni, N., Sadeghnia, H. R., Mobarhan, M. G., Movaffagh, J., Frade, M. L., Annunzio, S. R., Calixto, G. M. F., Victorelli, F. D., Chorilli, M., & Fontana, C. R. (2018). Assessment of chitosan-based hydrogel and photodynamic inactivation against *Propionibacterium acnes*. *Molecules*, 23(2), 1–16.
 - DOI: https://doi.org/10.3390/molecules23020473
- Firmino, H. C. T., Nascimento, E. P., Neves, G. A., & Menezes, R. R. (2017). Atividade antibacteriana de nanopartículas de óxido de cério. *Revista Eletrônica de Materiais e Processos*, 12(2), 64–95.
 - DOI: https://remap.revistas.ufcg.edu.br/index.php/remap/article/view/628/431
- Frade, M. L., Annunzio, S. R., Calixto, G. M. F., Victorelli, F. D., Chorilli, M., & Fontana. C. R. (2018). Assessment of chitosan-based hydrogel and photodynamic inactivation against propionibacterium acnes. *Molecules*, 23:2(1-16). DOI: https://doi.org/10.3390/molecules23020473
- Gao, M., Yao, J., Li, J., Su, R., Liu, Y., Chen, L., & Yang, J. (2021). A novel strategy for improving SERS activity by cerium ion f□d transitions for rapid detection of endocrine disruptor. *Chemical Engineering Journal*, 430, 131467. DOI: https://doi.org/10.1016/j.cej.2021.131467
- Ghasemiyeh, P., & Mohammadi-Samani, S. (2020). Potential of nanoparticles as permeation enhancers and targeted delivery options for skin: Advantages and disadvantages. *Drug Design, Development and Therapy*, 14, 3271–3289.
 - DOI: https://doi.org/10.2147/dddt.s264648
- Guo, L., Ping, J., Qin, J., Yang, M., Wu, X., You, M., You, F., & Peng, H. (2021). A comprehensive study of drug loading in hollow mesoporous silica nanoparticles: Impacting factors and loading efficiency. *Nanomaterials*, 11(5), 1293.
 - DOI: https://doi.org/10.3390/nano11051293

• Iole, G., Cione, E., Risoli, A., Genchi, G., & Ragno, G. (2005). Accelerated photostability study of tretinoin and isotretinoin in liposome formulations. *International Journal of Pharmaceutics*, 293(1–2), 251–260.

DOI: https://doi.org/10.1016/j.jpharm.2005.01.012

• Kargar, H., Ghazavi, H., & Darroudi, M. (2015). Size-controlled and bio-directed synthesis of ceria nanopowders and their in vitro cytotoxicity effects. *Ceramics International*, 41(3), 4123–4128.

DOI: https://doi.org/10.1016/j.ceramint.2014.11.108

• Khalil, K. M. S., Elkabee, L. A., & Murphy, B. (2005). Formation and characterization of different ceria/silica composite materials via dispersion of ceria gel or soluble ceria precursors in silica sols. *Journal of Colloid and Interface Science*, 287(2), 534–541.

DOI: https://doi.org/10.1016/j.vibspec.2019.102943

 Khalil, N. Y., Darwish, I. A., & Ahtani, A. A. (2020). Isotretinoin. Profiles of Drug Substances, Excipients and Related Methodology, 45, 119–157.

DOI: https://doi.org/10.1016/bs.podrm.2019.10.005

• Latif, M. M., Haq, A., Amin, F., Ajaz-Um-Nabi, M., Khan, L., & Sabir, N. (2021). Synthesis and antimicrobial activities of manganese (Mn) and iron (Fe) co-doped cerium dioxide (CeO₂) nanoparticles. *Physica B: Condensed Matter*, 600, 1–7.

DOI: https://doi.org/10.1016/j.physb.2020.412562

• Latter, G., Grice, J. E., Mohamed, Y., Roberts, M. S., & Benson, H. A. E. (2019). Targeted topical delivery of retinoids in the management of acne vulgaris: Current formulations and novel delivery systems. *Pharmaceutics*, 11(10), 490.

DOI: https://doi.org/10.3390/pharmaceutics11100490

• Luo, L. J., Nguyen, D. D., & Lai, J. Y. (2020). Dually functional hollow ceria nanoparticle platform for intraocular drug delivery: A push beyond the limits of static and dynamic ocular barriers toward glaucoma therapy. *Biomaterials*, 243, 119961.

DOI: https://doi.org/10.1016/j.biomaterials.2020.119961

• Machine, W. B. S., Enache, T. A., Jorge, A. M., & Oliveira-Brett, A. M. (2016). Isotretinoin oxidation and electroanalysis in a pharmaceutical drug using a boron-doped diamond electrode. *Electroanalysis*, 28(11), 2709–2715.

DOI: http://hdl.handle.net/11449/169146

- Matos, L. N. (2021). Síntese e caracterização de compostos de coordenação do ciprofibrato com Ca(II), Fe(II) e Ni(II). *Tese (Doutorado em Química)*, Universidade Federal de Goiás, Goiânia.
- Mendes, A. P. P. (2019). Cinética de liberação de clorexidina em nanocompósito de magnetita e quitosana. Dissertação (Mestrado em Química), Universidade Federal de São Carlos, São Carlos.
- Nourmohammadi, E., Oskuee, R. K., Hasanzadeh, L., Mohajeri, M., Hashemzadeh, A., Rezayi, M., & Darroudi, M. (2018). Cytotoxic activity of greener synthesis of cerium oxide nanoparticles using carrageenan towards a WEHI 164 cancer cell line. *Ceramics International*, 44(16), 19570–19575.

DOI: https://doi.org/10.1016/j.ceramint.2018.07.201

- Ogunjimi, A. T. (2018). Isotretinoin-loaded Delonix polymeric nanoparticles: Prospects as a delivery tool in the treatment of acne. *Tese* (*Doutorado em Ciências*), Universidade de São Paulo, Faculdade de Ciências Farmacêuticas de Ribeirão Preto, Ribeirão Preto.
- Ogunjimi, A. T., Chahud, F., & Lopez, R. F. V. (2021). Isotretinoin-Delonix polymeric nanoparticles: Potentials for skin follicular targeting in acne treatment. *International Journal of Pharmaceutics*, 610, 121217.

DOI: https://doi.org/10.1016/j.ijpharm.2021.121217

• Patel, M. R., Patel, R. B., Parikh, J. R., & Patel, B. G. (2011). Improving the isotretinoin photostability by incorporating in microemulsion matrix. *ISRN Pharmaceutics*, 2011, 838016.

DOI: https://doi.org/10.5402/2011/838016

Patel, R., & Prabhu, P. (2020). Nanocarriers as versatile delivery systems for effective management of acne.
 International Journal of Pharmaceutics, 579, 119140.

DOI: https://doi.org/10.1016/j.ijpharm.2020.119140

- Pawlaczyk, M., Pasieczna-Patkowska, S., Ryczkowski, J., & Schroeder, G. (2019). Photoacoustic infrared spectroscopic studies of silica surface functionalized by dendrimers. *Vibrational Spectroscopy*, 103, 102943. DOI: https://doi.org/10.1016/j.vibspec.2019.102943
- Periyat, P., Laffir, F., Tofail, S. A. M., & Magner, E. A. (2011). A facile aqueous sol-gel method for high surface area nanocrystalline CeO₂. RSC Advances, 1(9), 1794–1798. DOI: https://doi.org/10.1039/c1ra00524c
- Pop, O. L., Mesaros, A., Vodnar, D. C., Suharoschi, R., Tabaran, F., Magerusan, L., Todor, I., Diaconeasa, Z., Balint, A., Cionteam, L., & Socaciu, C. (2020). Cerium oxide nanoparticles and their efficient antibacterial application in vitro against gram-positive and gram-negative pathogens. *Nanomaterials*, 10(8), 1–15.

DOI: https://doi.org/10.3390/nano10081614

Rajeshkumar, S., & Naik, P. (2018). Synthesis and biomedical applications of cerium oxide nanoparticles – A
review. Biotechnology Reports, 17, 1–5.

DOI: https://doi.org/10.1016/j.btre.2017.11.008

- Rego, M. T. (2019). Obtenção, caracterização e avaliação da atividade antifúngica de nanopartículas de quitosana contendo o peptídeo TistH identificado na peçonha do escorpião *Tityus stigmurus*. *Tese* (*Doutorado em Ciências Farmacêuticas*), Universidade Federal do Rio Grande do Norte, Natal, RN.
- Roberts, M. S., Mohamed, Y., Pastore, M. N., Namjoshi, S., Youef, S., Alinagui, A., Haridass, I. N., Abd, E., Leite-Silva, V. R., Benson, H. A. E., Bellomo, R., Brunner, M., & Tadjally, E. (2021). New formulations of isotretinoin for acne treatment: Expanded options and clinical implications. *The Journal of Clinical and Aesthetic Dermatology*, 14(12 Suppl 1), S18.

DOI: https://pubmed.ncbi.nlm.nih.gov/35291260

• Sadhukahn, P., Kundu, M., Rana, S., Kumar, R., Das, J., & Sila, P. C. (2019). Microwave-induced synthesis of ZnO nanorods and their efficacy as a drug carrier with profound anticancer and antibacterial properties. *Toxicology Reports*, 6, 176–185.

DOI: https://doi.org/10.1016/j.toxrep.2019.01.006

• Sandrini, M., Gemelli, J. C., Gibin, M. S., Zanuto, V. S., Muniz, R. F., De Vicente, F. S., & Belançon, M. P. (2023). Synthesis and properties of cerium-doped organic/silica xerogels: A potential UV filter for photovoltaic panels. *Journal of Non-Crystalline Solids*, 600, 122033–122040.

DOI: https://doi.org/10.1016/j.jnoncrysol.2022.122033

• Schaffazick, S. R., Guterres, S. S., Freitas, L. L., & Pohlmann, A. R. (2003). Caracterização e estabilidade físico-química de sistemas poliméricos nanoparticulados para administração de fármacos. *Química Nova*, 26(5), 726–737.

DOI: https://doi.org/10.1590/S0100-40422003000500017

- Sharmila, G., Muthukumaran, C., Saraswarchi, H., Sangeetha, E., Soudarya, S., & Kumar, N. M. (2019). Green synthesis, characterization and biological activities of nanoceria. *Ceramics International*, 45(9), 12382–12386.
 - DOI: https://doi.org/10.1016/j.ceramint.2019.03.164
- Viossat, V., Lemoine, P., Dayan, E., Dung, N. H., & Viossat, B. (2005). Synthesis, crystal structures and IR spectra of isotypic pseudopolymorph complexes of Zn(II) by indole-2-carboxylic acid and 2,9-dimethyl-1,10-phenanthroline with different solvates (DMA, DMF or DMSO). *Journal of Molecular Structure*, 741, 45–52.

DOI: https://doi.org/10.1016/j.molstruc.2005.01.040

• Vyas, A., Sonker, A. K., & Gidwani, B. (2014). Carrier-based drug delivery system for treatment of acne. *The Scientific World Journal*, 2014, 276260.

DOI: https://doi.org/10.1155/2014/276260

• Wang, Y. Z., Wu, Y. S., Yang, H., Wang, M., Shi, X. G., & Zhang, W. S. (2018). Effect of calcination temperature on the microstructure and antimicrobial activity of boron and cerium co-doped titania nanomaterials. *Materials Technology*, 33(1), 48–56.

DOI: https://doi.org/10.1080/10667857.2017.1389051

• Wu, X., Landfester, K., Musyanovych, A., & Guy, R. H. (2010). Disposition of charged nanoparticles after their topical application to the skin. *Skin Pharmacology and Physiology*, 23(3), 117–123.

DOI: https://doi.org/10.1159/000270381

• Yap, K. L., Liu, X., Thenmozhiyal, J. C., & Ho, P. C. (2005). Characterization of the 13-cis-retinoic acid/cyclodextrin inclusion complexes by phase solubility, photostability, physicochemical and computational analysis. *European Journal of Pharmaceutical Sciences*, 25(1), 49–56.

DOI: https://doi.org/10.1016/j.ejps.2005.01.021

• Zaki, M. I., Hussein, G. A. M., Mansour, S. A. A., Ismail, H. M., & Mekmemer, G. A. H. (1997). Ceria on silica and alumina catalysts: Dispersion and surface acid-base properties as probed by X-ray diffractometry, UV-Vis diffuse reflectance and in situ IR absorption studies. *Colloids and Surfaces A: Physicochemical and Engineering Aspects*, 127(1–3), 47–56.

DOI: https://doi.org/10.1016/S0927-7757(96)03943-X

• Zhang, C., Yu, S., Tang, Z., & Guo, B. (2022). Catalyzed silanization by supporting ceria on silica towards rubber composites with improved mechanical properties. *Composites Communications*, 32, 101168.

DOI: https://doi.org/10.1016/j.coco.2022.101168

• Zhao, W., Wei, J.-S., Zhang, P., Chen, J., Kong, J. L., Sun, L. H., Xiong, H. M., & Möhwald, H. (2017). Self-assembled ZnO nanoparticle capsules for carrying and delivering isotretinoin to cancer cells. *ACS Applied Materials and Interfaces*, 9(22), 18474–18481.

DOI: https://doi.org/10.1021/acsami.7b02542

• Zholobak, N. M., Shcherbakov, A. B., Ivanova, O. S., Reukov, V., Baranchikov, A. E., & Ivanov, V. K. (2020). Nanoceria-curcumin conjugate: Synthesis and selective cytotoxicity against cancer cells under oxidative stress conditions. *Journal of Photochemistry and Photobiology B: Biology*, 209, 111921.

DOI: https://doi.org/10.1016/j.jphotobiol.2020.111921

©**2025 Braz WR**, et al. This is an open-access article distributed under the terms of the Creative Commons Attribution License 4.0 International License.

